Acoustics at the Nanoscale

Anthony Zander (1), Md Ayub (1), Benjamin Cazzolato (1), Carl Howard (1), Md Julker Nine (2), Dusan Losic (2), David Huang (3), Diana Tran (2), and Hywel Bennett (1)

(1) School of Mechanical Engineering, The University of Adelaide, SA 5005, Australia
(2) School of Chemical Engineering, The University of Adelaide, SA 5005, Australia
(3) Department of Chemistry, School of Physical Sciences, The University of Adelaide, SA 5005, Australia

ABSTRACT

This article provides an overview of recent research on acoustics at the nanoscale including how recent developments in nanotechnology are being utilised to create advanced acoustic materials that incorporate either carbon nanotubes or graphene as components. Methods to overcome the challenges involved in conducting experimental measurements on relatively small samples to characterise the acoustic performance of the developed acoustic materials are detailed. The acoustic performance of the developed materials is presented and the hypothesised mechanisms for their enhanced performance are described. The simulation tools applicable to modelling acoustics at the nanoscale have been outlined as well as the challenges faced in modelling the acoustic performance of the developed acoustic materials in the audible frequency range and approaches currently being developed to address these challenges.

1 INTRODUCTION

Noise is a common problem in almost every engineering application incorporating a mechanical device or fluid motion that can act as a noise generating source, such as home appliances, engine vibration, buildings, vehicles, and aircraft (Crocker and Arenas 2007; Arenas and Crocker 2010). Numerous research studies have been conducted to introduce new materials and methods for noise control engineering (Hong *et al.* 2007; Robinson 2008; Leroy *et al.* 2008). Interest in nanoscale materials has grown rapidly with the advances in nanotechnology in which the dimensions of the structures and devices are on the order of a few nanometer, where a nanometer is equal to a billionth of a meter (10^{-9} m). Visual inspection of such materials requires electron microscopy as the characteristic length of these materials is in the nanometre range and thus not within the range of human visual acuity. For instance, Figure 1(a) shows the molecular structure of a carbon nanotube which has a diameter of the order of a nanometre and is almost 50,000 times smaller than the diameter of a human hair. Advances in nanotechnology have provided researchers with a number of new materials comprising nanofibers or nanopores that can potentially be implemented as acoustic absorption materials. The molecular behaviour of these new nanoscale materials may have a significant influence on their sound absorption and their extraordinary properties could play an important role in reducing the thickness and mass of acoustic absorbers compared with currently available materials.

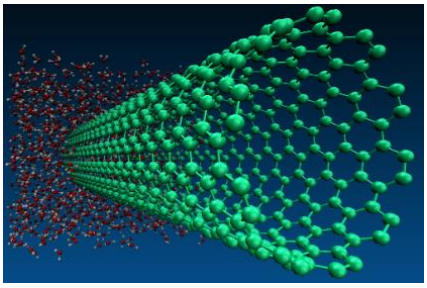

(a)

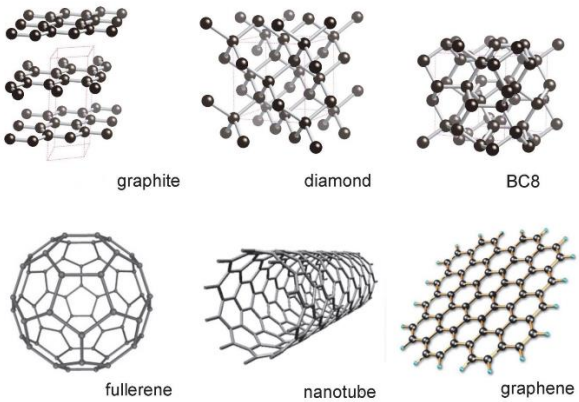

(b) Source (Oganov et al., 2013)

Figure 1: (a) Atomic structure of a carbon nanotube (CNT); (b) Selected allotropes of Carbon.

A variety of nanomaterial constituents are available that can be formed into nanoscopic fibres. In particular, carbonaceous materials are currently under intensive research for various applications including advanced energy conversion and energy storage devices due to the emergence of various nanomaterials with favourable nanostructures and their large surface/interface area. Carbonaceous materials can be found in the form of several allotropes of carbon as shown in Figure 1(b). Of particular interest are materials based on graphene which is a monolayer of carbon atoms in a densely-packed two-dimensional (2D) honeycomb crystal structure (Tiwari and Syväjärvi, 2015), and carbon nanotube, a one-atom thick wall of graphene rolled up into a seamless cylinder with a diameter of the order of a nanometre. These have received considerable attention due to their exceptional properties such as high thermal conductivity, high electrical conductivity, high transparency, great mechanical strength, inherent flexibility, high aspect ratio and large surface area (Liu *et al.* 2012). Many of their properties are still being explored and novel ways in which these nanoscale structures can be used are being discovered at an astounding rate.

Since the discovery of the carbon nanotube (CNT) structure by Iijima (1991), numerous potential applications for CNTs have been suggested in the fields of electronics, energy, mechanics, field emission and lighting. Consequently, considerable research investment has been made to realise new functionalities such as high damping (Xu *et al.*, 2010), near-ideal black-body absorption (Mizuon *et al.*, 2009) and thermoacoustic sound emission (Xiao *et al.* 2008). Fabrication of these materials with modified mechanical and thermal properties show promise as sound-absorption materials for noise control (Ajayan *et al.*, 2006; Cho *et al.*, 2014a; 2014b). Hence, the potential of using CNTs and composite absorbers for noise-control applications has been investigated in various studies. Qian *et al.* (2014) have shown that super-aligned CNTs grown on the surface of a micro-perforated panel (MPP) surface can improve the acoustic absorption performance of MPP absorbers at low frequencies. Investigations have also been conducted for a nano-integrated polyurethane foam using multi-walled CNTs (Cherng, 2006). Test results showed that the integration of CNTs improved the acoustic absorption performance by 5-10% in the frequency range 800-4000 Hz. CNTs incorporated into flexible polyurethane (PU) foams up to 0.20 wt% have also been reported to enhance the absorption performance of these conventional porous materials (Bandarian *et al.*, 2011; Verdejo *et al.*, 2009; Basirjafari *et al.*, 2012). It was suggested that the nanotubes may improve the sound absorption performance of the polymer nanocomposites as the individual nanotubes oscillate with the sound waves, helping further absorb sound energy (Crawford, 2012). These developments in nanotechnology offer exciting possibilities for developing acoustic absorption materials using nanotubes.

Similarly, the potential of graphene is still being explored with the development of 3D graphene-based structures and the exploration of other novel ways in which the nanostructures can be used for various applications (Li and Qiu, 2014). Recent progress in advanced manufacturing offer exciting possibilities in fabricating porous nanostructures of graphene and their composites such as Graphene foam (Sun *et al.* 2016), Graphene aerogel (Zhang *et al.* 2016), CNT/Graphene sandwich (Tang *et al.* 2014), CNT-graphene hybrid layer (Zhu *et al.* 2012) and a more recently developed directionally antagonistic graphene oxide-polyurethane hybrid aerogel (Oh *et al.*, 2018). With nanopore structures, high porosity and inherently flexible frames which are effective for energy dissipation thud have high potential for development as thin acoustic absorbers (Tiwari and Syväjärvi 2015, Fan *et al.* 2010, Zhang *et al.* 2013). Development of materials comprising graphene-based nanocomposite porous structures can potentially have advantages for sound absorption mechanisms as they can allow energy transfer through an open-cell connecting structure that can transfer the energy into and from the gas in the pores and also with the elastic (limp) frames of the solid matrix (Kuczmarski and Johnston 2011).

However, a fundamental understanding of the physical mechanisms associated with the use of nanomaterials acting as acoustic absorbers and their potential benefits has not as yet been developed. The current research aims to investigate the mechanisms of sound absorption at the nanoscale, and examine the potential of using novel arrangements of nanomaterials which have been optimised for sound absorption to create acoustic absorbers that achieve a high level of sound absorption using a very thin layer of material. This application of nanotechnology is expected to lead to the development of new sound absorbing materials that are better performing and more compact than existing materials. Potential applications include aircraft jet engine nacelle liners, where in addition to reduced noise, more compact acoustic absorbers would permit a smaller engine nacelle, which would in turn reduce drag and provide fuel savings; and other acoustic devices such as duct liners, mufflers, and absorptive blankets. Acoustic absorber materials have application essentially anywhere that noise exists and needs to be attenuated. Future developments could also include underwater applications such as acoustic tiles for the next generation of submarines.

2 MEASUREMENT OF ACOUSTIC ABSORPTION PERFORMANCE

The performance of acoustic absorbers is quantified by their acoustic absorption coefficient which is the ratio of the sound intensity attenuated and the intensity of the sound incident upon the absorber. The acoustic absorption coefficient can be measured using either the reverberant room method or the impedance tube method (Robin *et al.*, 2014). The impedance tube method can be used to measure the normal incidence sound absorption on small samples and the reverberant room method allows measurement on larger samples with diffuse acoustic field excitation (Robin *et al*., 2014). For this study, the absorption coefficient of the naturally small nanomaterial samples was measured in an impedance tube using two microphones in accordance with the ASTM standard (ASTM E 1050; Chung & Blaser, 1980a; 1980b).

2.1 Impedance tube apparatus

A custom made Ø25.40 mm copper impedance tube was used to measure the normal incidence acoustic absorption coefficient of the carbon nanotube sound absorber. A schematic and photograph of the experimental apparatus are shown in Figure 2. The instrumentation compromised two ¼ inch Brüel & Kjær (B&K) array microphones type 4958, a four channel B&K Photon+™ data acquisition system and LDS Dactron software (LDS Group 2013). The B&K microphones have a free field frequency response (re 250 Hz) of ±2 dB within the frequency range 50 Hz to 10 kHz. A B&K type 4231 acoustic calibrator was used to calibrate the microphones to 94 dB at 1 kHz. Measurement data was acquired to give a 4 Hz frequency resolution, with a sampling interval of 7.60 µs (with 12800 lines and 32768 points) and sample records of finite duration of approximately 106 s for 300 averages using a Hanning window. The standard microphone-switching technique (Chung & Blaser 1980a; Katz 2000) was implemented to calibrate the microphones used in the impedance tube, which ensured that any variation in the magnitude and phase of the measured transfer function due to the differences in the two sensors was eliminated. During the measurement, it was identified that due to its small diameter the tube has significant attenuation and performs as a lossy waveguide. Hence, an additional correction, using a method developed by Han *et al.* (2007), was also applied to account for the tube attenuation due to viscous and thermal losses at the tube walls, as well as damping and leaks. Details of these corrections and the impedance tube method can be found in previous work (Ayub *et al.* 2017; Han *et al.* 2007).

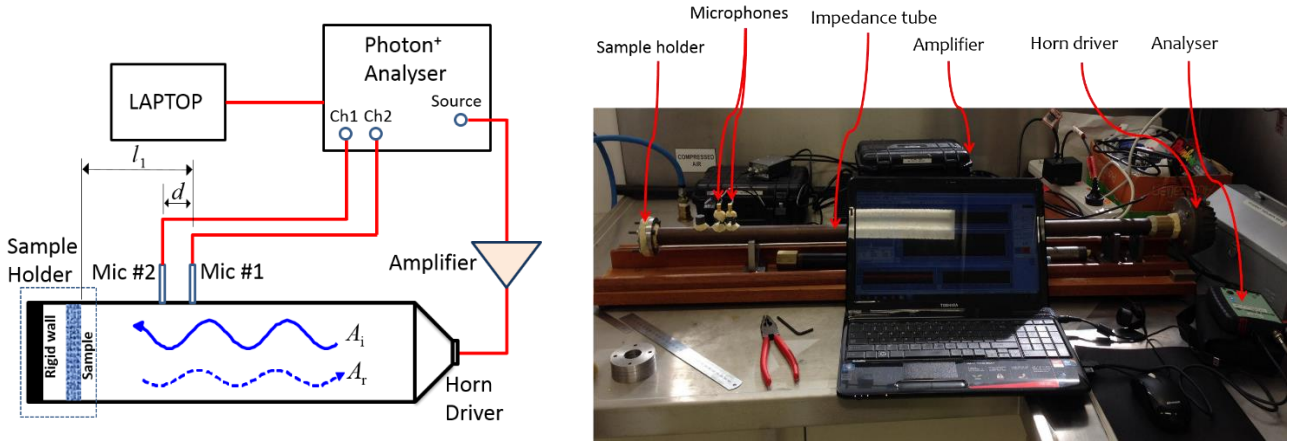

(a) (b)

Figure 2: (a) Schematic and (b) photograph of impedance tube and instrumentation used to measure the absorption coefficient of the fabricated acoustic absorber samples.

3 NANOMATERIAL BASED ACOUSTIC ABSORBERS

Our research to date on acoustics at the nanoscale includes advanced acoustic absorbers that incorporate either carbon nanotubes or graphene. The experimental investigation of the acoustic absorption behaviour of these nanomaterial based acoustic absorbers are conducted using the impedance tube comprised measurements of the normal incidence sound absorption coefficient of the test samples up to a maximum frequency of 4.2 kHz. The measured coherence between the acoustic source and the microphone signals for the tests conducted here was found to be close to 1 for the majority of the frequency range from 125 Hz–4 kHz. Hence, results are presented here for only that frequency range.

3.1 Carbon nanotube (CNT) acoustic absorber

Carbon nanotubes can be produced with an average diameter in the range of 3–50 nm and typical lengths of 10 µm to hundreds of micrometres (Seetharamappa, 2006) and more recently even millimetre lengths (Cho *et al.*, 2014a, 2014b) and thus can be used to produce absorbers with nanopores (Ajayan *et al.*, 2006). Open pore structures, together with the nanopores of the tubes, can potentially enhance the acoustic absorption of CNT absorbers. Recent improvements in the fabrication of CNT absorbers with various CNT forest densities (Cho *et al.*, 2014a; 2014b) suggests arrangements of carbon nanotubes that are optimised for acoustic absorption. In this study, vertically aligned carbon nanotube forests grown on silicon wafer substrates were used as samples to study the behaviour of CNT acoustic absorbers. The CNT samples used in this study were manufactured by a research team in the Nanoworld Laboratories at the University of Cincinnati, USA. Each sample was 3 mm thick and cut to have the same circular diameter of 25.40 mm to match the internal diameter of the impedance tube. The bulk density of the sample was calculated as $\sigma_{3mm\ CNT}$ = 43.40 kg m^{-3}. A photograph of the 3 mm CNT forest grown on the substrate is shown in Figure 3. Details of the manufacturing method and reaction condition during the fabrication of the CNT forest can be found in previously published works (Ayub *et al.* 2017; Cho *et al.* 2014a; 2014b).

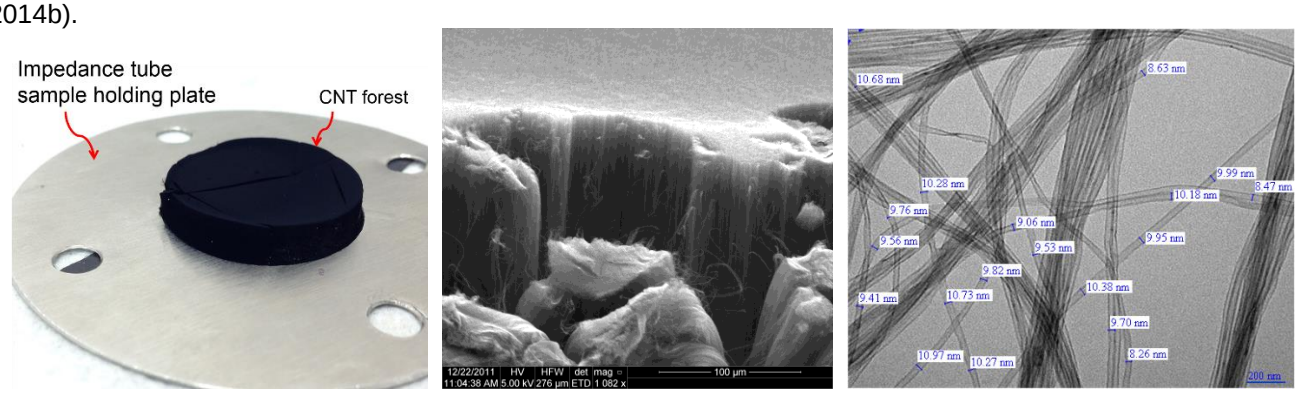

(a) Fabricated CNT sample (b) SEM image (c) TEM image

Figure 3: (a) Fabricated sample of 3mm forest of CNT arrays; (b)SEM image of the CNT forest near the edge of the sample showing the vertical arrangement of the tubes on the substrate; (c) TEM image of the disperse carbon nanotubes showing the tube diameter.

The micro-morphological surface features were examined using a scanning electronic microscope (SEM) and a transmission electron microscope (TEM) to provide the characterisation of the samples such as length and diameter of the CNTs, number of tubes per unit area and tube orientation. The arrangement of the tubes in the absorber sample can be observed from an SEM image of the fabricated CNT samples shown in Figure 3(b). The average diameter of the nanotubes in the sample can be measured using a TEM image of dispersed CNTs shown in Figure 3(c), which was estimated at approximately 8 nm.

3.1.1 Acoustic absorption behaviour of CNT absorber

The acoustic absorption performance of CNT forests can be compared with that of conventional materials such as melamine foam and glass wool for an equivalent thickness or mass. The analytical framework applied here was adapted from Kino and Ueno (2008) to predict the normal incidence acoustic absorption coefficient of a reference thickness of 25.5 mm melamine foam and 25 mm of glass wool using the relevant non-acoustical parameters. Thereafter, the model was used to predict the acoustic absorption coefficient of both materials by reducing the material thickness to 3 mm, equivalent to that of the CNT forest. Comparison of the absorption coefficient of the 3 mm CNT forest and conventional porous materials of equivalent thickness is displayed in Figure 4(a), which shows that both conventional materials considered here exhibit lower absorption than the CNT forest for an equivalent thickness. A similar comparison of the acoustic absorption coefficient of the CNT forest and the porous materials is presented in Figure 4(b) for an equivalent mass to the CNT sample (0.0499 g). It can be observed that 4.09 mm of glass wool of equivalent mass (0.0499 g) may provide similar absorption to a 3 mm CNT forest. On the other hand, 12.63 mm of melamine foam of equivalent mass may yield a maximum absorption of 50% (at 4 kHz) over the measured frequency range, which is significantly higher than the CNT forest. As shown in Figure 4(b), even though an equivalent mass of melamine foam may produce significantly higher sound absorption than that of a CNT forest, it is four times as thick as the CNT forest. These results highlight the significance

of the absorption ability of CNTs and their potential for implementation in CNT acoustic absorbers, particularly in applications where the thickness of the absorber is of primary consideration.

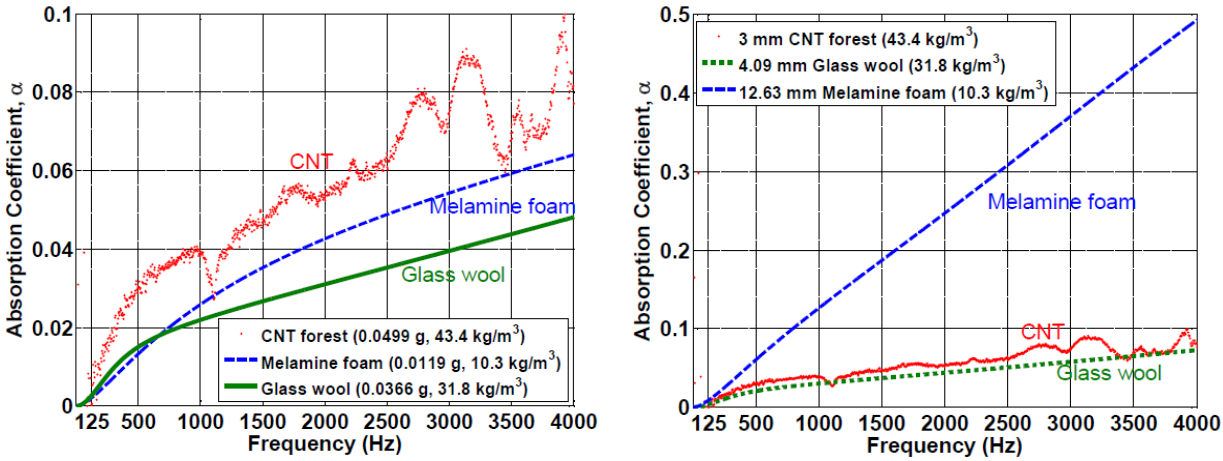

(a) Equivalent thickness (3 mm) (b) Equivalent mass (0.0499 g)

Figure 4: Comparison of experimentally measured acoustic absorption coefficient of CNT forest with theoretical estimates for two conventional porous materials, melamine foam and glass wool, of equivalent (a) thickness (3 mm) and (b) mass (0.0499 g). Note that the mass of CNTs (without the substrate) here is an estimate from the sample configuration shown in Figure 3(a), in which the CNTs were attached to the substrate.

3.2 Graphene acoustic absorber

Many commercially used acoustic absorbing materials (such as natural fibres, melamine foams) are hydrophilic by nature and hold moisture in their structure which can possibly lead to bio-deterioration of the material, with significant economic loss for their maintenance and replacement (Viitanen *et al.*, 2009; Dedesko & Siegel, 2015). Consequently, the strong commercial demands for fire-proof acoustic absorbers limit the use of many natural and synthetic acoustic materials due to their poor fire-retardancy (Fatima & Mohanty, 2011). To address the combined challenges of achieving enhanced acoustic absorption, mechanical robustness, moisture insulation and fire-retardancy, we have developed a new approach to engineer the internal structure of conventional cellular acoustic absorptive materials using interconnected graphene oxide (GO) sheets. The concept is based on the creation of a unique lamella network using self-assembled GO sheets in a grill-shaped cellular skeleton to create optimal air-flow resistance and tortuosity, which is schematically illustrated in Figure 5. Melamine foam (MF) was chosen as the structural support because of its highly porous and well-structured limbs (Kino & Ueno, 2008), that interacts well with negatively charged GO and holds self-assembled interconnected films (Nine *et al.*, 2017a; 2017b). The self-assembled properties of GO facilitates microscopic sheets (~20 μm^2) to form into a macroscopic film (~0.01 mm^2) providing an edge-to-edge coverage of a large pore of MF that is apparently 500 times greater than the area of GO sheets used. This unique and randomly structured 3D-lamella provide tunable open and closed cell ratios to control the porosity and tortuosity of the structure for excellent noise absorption. A series of tests were performed to investigate the structural and morphological advantages of the developed materials for enhanced sound absorption, mechanical stiffness, humidity insulation, and fire-retardancy.

3.2.1 Preparation of GO assisted lamella structure with melamine foam

The conventional melamine foam (MF) was cut into pieces with a round sharp-edged punch of 26.5 mm in diameter to match with the impedance tube. The highly stable nematic phase of aqueous GO was used to load the melamine skeleton. The pieces of melamine foam were soaked in dimethylformamide before dipping into the aqueous GO for easy access of GO into the open cell-network for homogeneous distribution. Finally, the MF filled with homogenously distributed GO was dried at 50 °C in an oven for 12 h. The typical structures of the MF before and after the formation of lamella is presented in Figure 6. The self-assembly of microscopic GO sheets (~20 μm^2) forming into macroscopic films and in-situ limb-to-limb connections have been observed after the low temperature curing process as shown in Figures 5 and 6. Cross sectional SEM images made across vertical and horizontal directions showed the self-assembled GO film connected to the melamine limbs in the grill-shaped skeleton which covered an approximate area of ~0.01 mm^2 as shown in Figure 5(c-e).

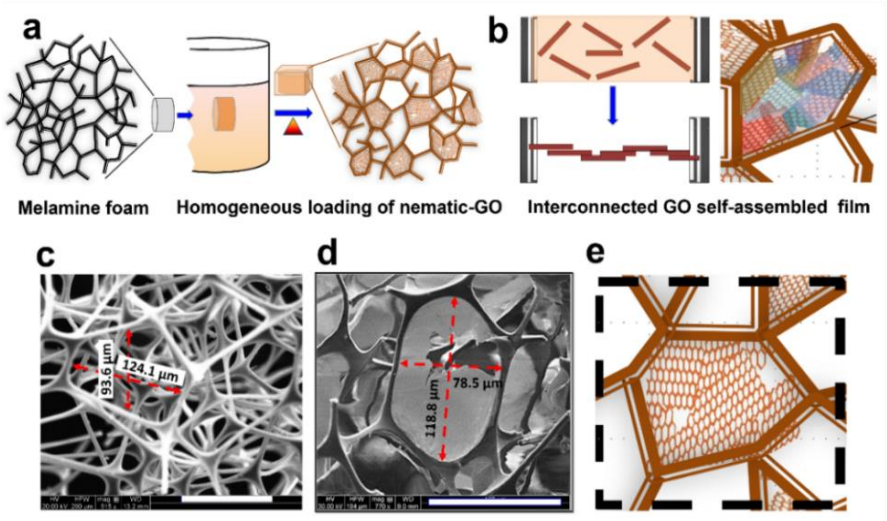

Figure 5: (a) Schematic presentation of synthesis of the GO-lamellar structure in melamine skeleton, (b) self-assembly of microscopic GO sheets to macroscopic interconnected GO film forming lamellar structure, (c) Lateral distance between limbs of the melamine skeleton. (d, e) Self-assembled interconnected GO film in MF cell and schematic of the macroscopic GO film forming a closed cell.

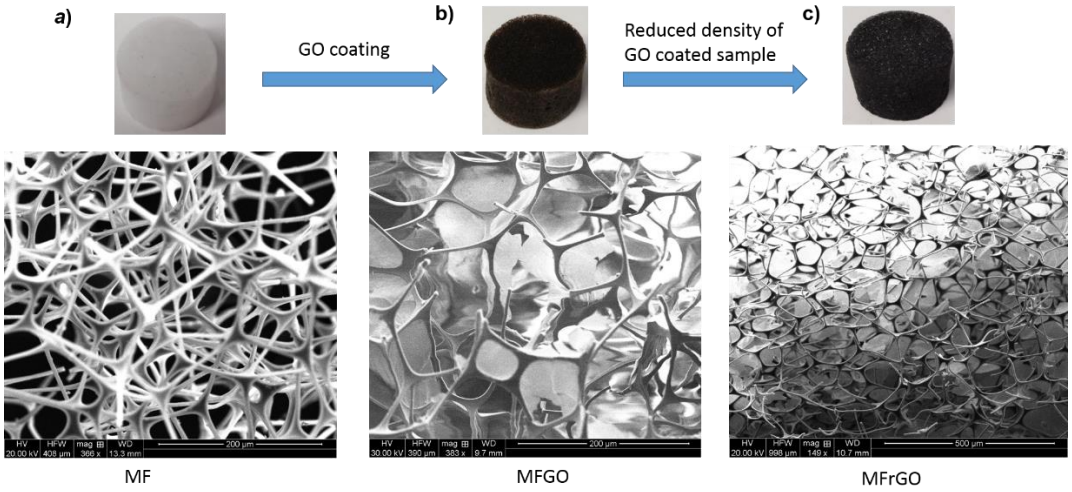

Figure 6: Fabricated samples of a) uncoated melamine foam (MF), b) GO coated melamine foam (MFGO), c) reduced GO foam (MFrGO) and their corresponding SEM images showing random blocks of GO flakes developed inside the foam skeleton.

The density of the lamella structures based on the self-assembly of GO sheets into the MF skeleton is tuneable by loading the percentage of nematic-GO. This was controlled by using a different concentration for GO and repetition of the cycle to obtain different densities of GO coated melamine foam (MFGO) samples. The MFGO samples with different densities (five densities- denoted as MFGO-1 to 5) were reduced in two steps to observe the change in relevant properties of the lamella structure which includes weight, density, and wettability of the structure. Step 1 involves reduction of the MFGO samples using hydrazine vapor followed by Step 2 of thermal annealing at 160 °C in a vacuum oven for 6 h. The photographs and the corresponding SEM images of the MF, MFGO and MFrGO (after reduction) samples at different stages of the fabrication process are shown in Figures 6(a) to 6(c).

3.2.2 Acoustic absorption behaviour of graphene oxide composite absorbers

Open-celled melamine foam usually provides behaviour good absorption performance in the mid to high frequency range. The absorption performance of the foam can be improved further through chemical modification of the foam using a graphene oxide (GO) suspension while maintaining the same material thickness and changing the bulk density of the materials. As shown in Figure 7(a), the acoustic absorption of melamine foam can be enhanced by up to 10% in the frequency range above 1500 Hz using graphene oxide (GO) coating with a loading as low as 20 mg in the foam (MFGO-1, total density of 12.39 kg/m^3) and with the same material thickness. Absorption can be enhanced further in the lower frequency range by increasing the GO loading in the foam. The absorption can be increased by up to 60% (as shown in Figure 7(c)) in the broadband frequency range between 500 Hz to 3500 Hz for MFGO sample density of 24.12 kg/m^3 (MFGO-5). It can also be observed that the reduced samples of MFrGO (i.e. removal of oxygen functional group and thus reduced density of MFGO samples) showed an absorption trend similar to the nonreduced MFGO samples with no significant changes in the absorption peaks as presented in Figure 7(c). As can be seen in Figure 7(a), the sound absorption is doubled from the control-MF (uncoated MF, 9.84 kg/m^3) with the highest density sample (MFGO-5) at some frequencies. The increase in loading percentage of GO also shows an almost linear increase in acoustic activity (Basirjafari *et al.* 2012), which provides a single measure of the absorption over a broad frequency range, as presented in Figure 7(b). In addition the GO loading shifts the highest absorption peaks towards the lower frequency making it suitable for low frequency sound absorption applications. Further proof of the enhancement of acoustic absorption performance at the low frequencies with the implementation of the impregnation of the GO material can be observed in the results of MFGO samples of larger thickness (39±1 mm) presented in Figure 7(d).

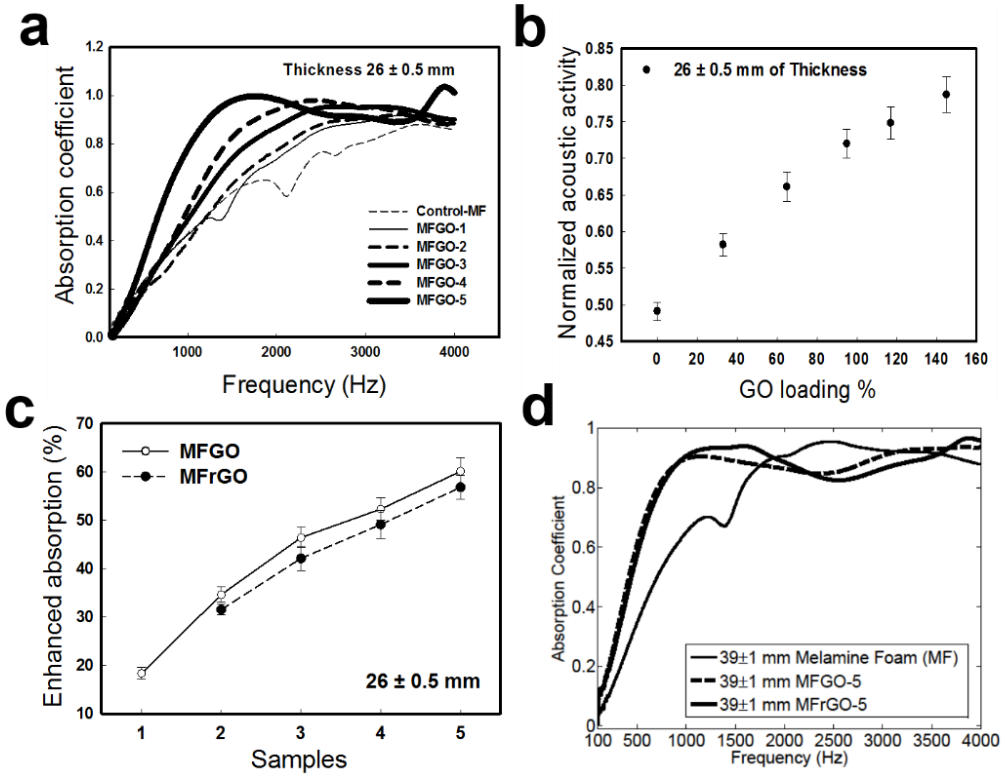

Figure 7: Acoustic absorption performance of GO assisted lamellar structure, (a). Acoustic absorption of MFGO samples of five different densities (12.39, 15.68, 18.77, 21.41, and 24.12 kg/m^3 denoted as MFGO- 1 to 5, respectively) compared with the control-MF for a thickness of 26±0.5 mm. (b). Acoustic activity (normalised acoustic absorption coefficient) based on percentage of GO loading. (c). The enhancement (% increase in acoustic activity) of acoustic absorption of lamella structures for both MFGO and MFrGO (reduced MFGO) samples (26 mm thickness) compared with control-MF. (d). Absorption performance of untreated (control-MF) and GO treated melamine foams (MF).

The outstanding sound absorption performance of these new structures is principally attributed to the air-flow resistance developed by the GO-based lamella structures. The air flow resistance is governed by the structural properties of absorption material which includes porosity, pore size, tortuosity and thickness. In the case of the MFGO samples, the interconnected GO thin film randomly blocks the pores inside the melamine skeleton (Figure 8), which changes the wave propagation path and thus significantly increases the tortuosity and slightly reduces the porosity of the material. This results in the increased flow resistance exhibited by all MFGO and MFrGO structures. Hence, the GO lamella structures in this study possessed high airflow resistance and correspondingly exhibited the enhanced acoustic absorption which is much higher than that of open cell structures. An illustration of this absorption phenomenon is shown in Figure 8.

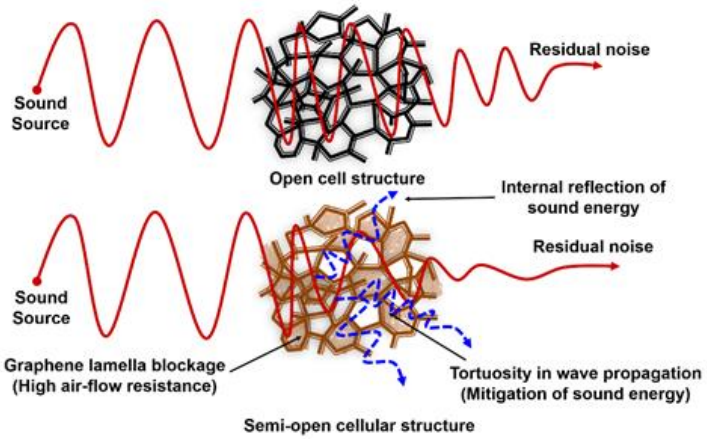

Figure 8: Schematic of acoustic propagation through open cell MF structure and semi-open cell (GO foam) lamella structures

3.2.3 Enhanced moisture insulation and fire-retardant properties

When incorporated into building structures sound absorption materials are required to provide moisture insulation and fire-retardant properties. In general, MF and GO are hydrophilic and prone to moisture entrapment in the structure, which may have negative impacts on the building structure, such as the growth of moulds and fungi in highly humid conditions (Viitanen *et al.*, 2009). Therefore, MFGO samples were reduced to not only achieve superior moisture insulation, and fire-retardancy but also to reduce their weight as well as making them highly stable (Turgut *et al.*, 2017). The reduced MFGO samples (denoted as MFrGO) exhibited outstanding moisture repellent properties, are light weight (density reduction) and possess fire-retardant properties as shown in Figures 9 and 10.

The hydrophilic melamine skeleton with the inclusion of GO showed an enhanced water contact angle of CA~104°, which further became superhydrophobic (super water repellent) showing a water contact angle of ~155° after the reduction process as shown in Figure 9. The self-assembly of GO lamella sheets in the MF structure enables it to resist moisture penetration by creating an impermeable barrier layer. Hence, the analysis of moisture absorption and desorption of the MFGO-3, and MFGO-5 samples including their reduced derivatives revealed excellent moisture insulation that provided almost 4-5 times better moisture insulation compared to Control-MF as shown in Figure 9(b). The superhydrophobic MFrGO samples outperform Control-MF and MFGO samples in both the absorption and desorption cycle (Figure 9(b)-(c)).

The thermal stability and flammability of the two representative samples (MFGO-3 and MFrGO-3) were investigated compared with Control-MF. The reduction of GO in MFrGO-3 sample showed higher thermal stability in comparison to the Control-MF and GO modified sample (MFGO-3). The thermogravimetric analysis of the samples showed that MFGO-3 sample lost mass in two stages between 150 °C and 400 °C, whereas only a single step mass loss was identified for MFrGO-3 sample at 350 °C. The thermal instability of non-reduced MFGO-3 samples was due to the abundant oxygen functional groups in the structure that were reduced to provide structural stability, which has also been confirmed by the volume of residue left after combustion. Moreover, the use of GO

without further reduction was found to possess an explosive fire hazard due to its possible flammability. The self-explosive behaviour of GO film was mitigated by reduction of MFGO lamella structure for enhanced stability during fire as shown in Figure 10. Therefore, the MFrGO samples are an effective acoustic absorber that are superhydrophobic, have low density, high thermal stability and enhanced sound absorption.

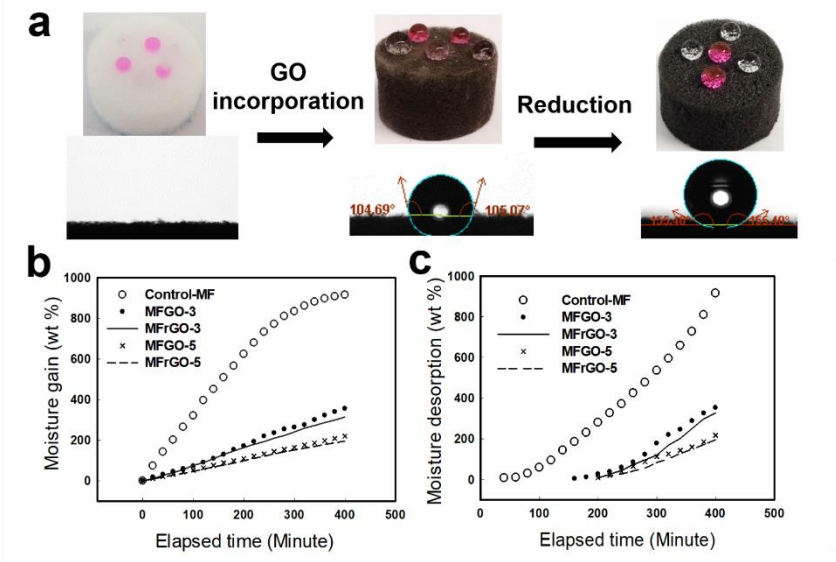

Figure 9: Wettability and mist absorption/desorption of the samples before and after reduction. a) Change in wettability of Control-MF, MFGO-3, and MFrGO-3 samples. (b,c) Mist absorption and desorption of MFGO and MFrGO samples compared to Control-MF.

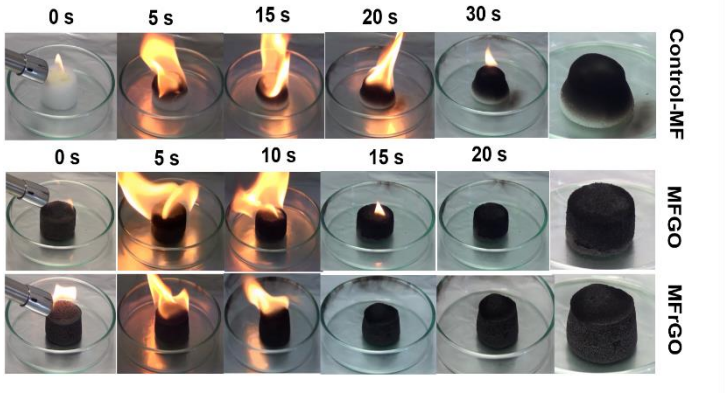

Figure 10: Flammability of the samples before and after reduction. Digital photographs of the burning test showing high temperature stability and fire-retardant properties of the samples in the presence of gasoline (10 µL).

3.2.4 Material thickness and mass requirements

The developed GO assisted lamellar structure are based upon an open-celled foam (such as melamine foam, polyurethane foam) impregnated with a graphene oxide (GO) coating. This changes the bulk density of the material, thus increasing the weight of the material. However, the novelty of the GO coated material is that it can provide similar acoustic absorption over a wide frequency range to an equivalent mass of an uncoated foam but with a reduction of 50% in the material thickness. Additionally, the MFGO material can be chemically treated to remove oxygen functional groups and moisture from the GO structure, as mentioned in Section 3.2.1, which makes the resulting MFrGO material up to 30% reduced density in comparison to the GO foam. As shown in Figure 7(c), open celled foam with reduced graphene oxide (MFrGO) can provide a light weight material by reducing 30% of the mass (density) in comparison to a GO-coated foam of equivalent thickness and equivalent acoustic absorption. In addition, at mid to high frequencies the MFrGO foams can provide absorption performance

equal to uncoated foams for an equivalent mass of the absorber with a reduction of 50% in the material thickness. For an equivalent thickness and mass, both GO and r-GO coated materials (MFGO and MFrGO) can provide improved acoustic absorption performance compared with the uncoated materials as shown in Figure 11. A comparison of these absorption performances can be seen in Figure 11.

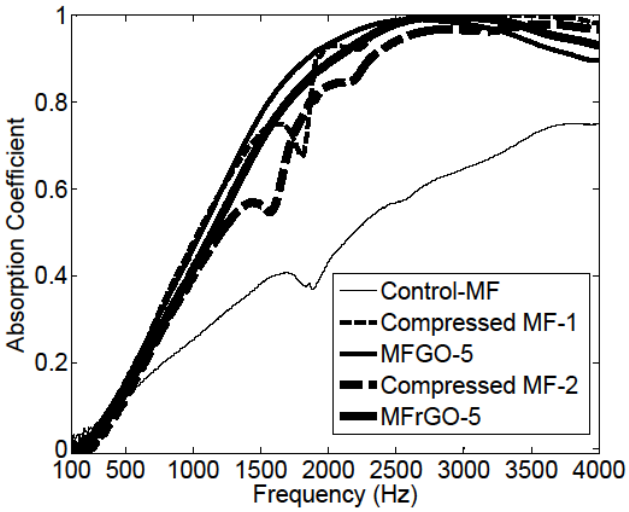

Figure 11: Effect of GO and r-GO on sound absorption for an equivalent absorber thickness of 18±0.5 mm and for equivalent masses (density) of MFGO-5 (24.12 kg/m^3) and MFrGO-5 (18.09 kg/m^3). MF-1 and MF-2 are melamine foams that were compressed to create samples of untreated foam of equivalent thickness (18±0.5 mm) and mass (24.12 kg/m^3 and 18.09 kg/m^3) to MFGO-5 and MFrGO-5, respectively.

4 NANOSCALE MODELLING FOR ACOUSTICS

The mechanisms of sound absorption for conventional porous acoustic materials with fiber diameters or pores on the micro-scale (down to 1 µm) are currently well understood. The relative influence of the various mechanisms are, however, expected to change for materials with pores or fibers at the smaller nanoscale (down to 1 nm), while other mechanisms and nonlinear effects may also become significant. Therefore, modelling acoustic mechanisms at the nanoscale requires molecular simulations that can model the flow behavior in the transition regime (Hadjiconstantinou & Garcia, 2001; Hadjiconstantinou, 2002), because the characteristic length scale of the nanoscale structures is comparable to the molecular mean free path, and hence the commonly used acoustic assumptions, such as continuity, are invalid (Ayub *et al.*, 2011). In addition, it is very important that a viable molecular simulation approach was chosen that can be employed to model all relevant and likely physical phenomena, namely fluid/structure interactions, bi-directional heat transfer, and acoustic wave propagation, associated with the interactions between the acoustic wave and the nanomaterial at the nanoscale. A study (Ayub *et al.*, 2011; 2013) of various molecular approaches of non-continuum methods indicated that molecular dynamics (MD) is the method best suited to simulate all relevant physical phenomena (illustrated in Figure 12) and study the acoustic absorption at the nanoscale.

4.1 Molecular Dynamics (MD)

Molecular dynamics (MD), a deterministic molecular simulation model, was employed to study sound wave propagation in an environment where the effects of acoustic absorption, relaxation, nonlinearity, fluid/structure interactions, and bi-directional heat transfer with a nanomaterial must be modelled simultaneously. Acoustic modelling at the nanoscale using MD was found to be useful to develop an understanding of the acoustic absorption mechanisms of the nanoscopic fibres (Ayub *et al.*, 2015).

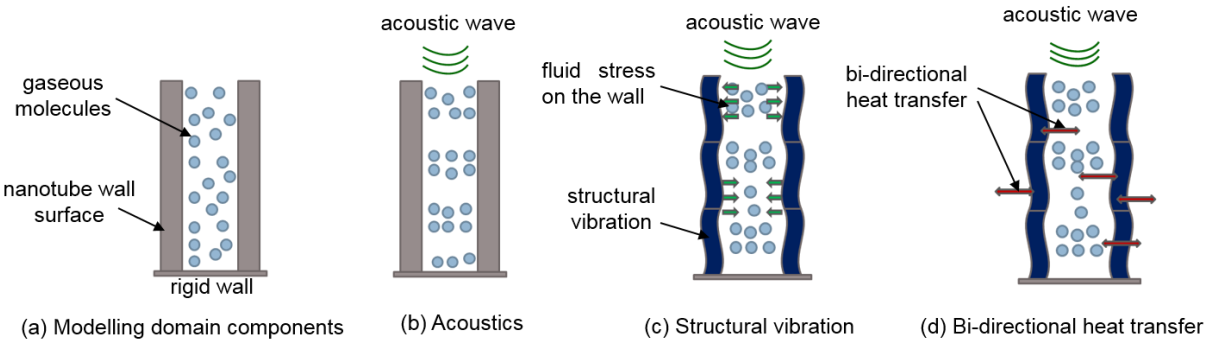

Figure 12: Schematics of physical phenomena required for acoustic flow modelling.

4.1.1 Basics of MD and force potentials

The basic working concept of molecular dynamics (MD) simulations is to generate particle trajectories in a microscopic system of interacting particles by solving Newton's equations of motion (Li 2005; Allen 2004; Hofmann 2003). All macroscopic quantities like pressure and temperature in the system can be described in terms of positions and velocities of individual molecules or atoms interacting with each other for a specified inter-particle interaction potential $U(\mathbf{r}^N)$ (Li 2005; Allen 2004; Hofmann 2003). For a simple atomic system, the classical equations of motion to calculate the forces $\mathbf{F}_i$ acting on the atoms may be written in terms of the interaction potential as

$$\mathbf{F}_i(\mathbf{r}^N) = -\nabla_i U(\mathbf{r}^N) = m_i \ddot{\mathbf{r}}_i = m_i \frac{\partial \dot{\mathbf{r}}_i}{\partial t}, \tag{1}$$

where $\mathbf{r}^N = (\mathbf{r}_1, \mathbf{r}_2, \mathbf{r}_3 \ldots \mathbf{r}_N)$ represents the complete set of 3N atomic coordinates, $\mathbf{F}_i = (\mathbf{F}_{ix}, \mathbf{F}_{iy}, \mathbf{F}_{iz})$, $\nabla_i \equiv (\frac{\partial}{\partial x_i}, \frac{\partial}{\partial y_i}, \frac{\partial}{\partial z_i})$, $\ddot{\mathbf{r}}_i \equiv \frac{\partial^2 \mathbf{r}_i(t)}{\partial t^2}, \dot{\mathbf{r}}_i \equiv v_i \equiv \frac{\partial \mathbf{r}_i(t)}{\partial t}$. The potential $U(\mathbf{r}^N)$ can be parameterised to represent the generic physical properties of molecules or atoms or to match the quantum calculations or experimental values of known properties of molecular systems of interest. The trajectory of the atoms is propagated numerically based on the forces acting on the atoms derived from the potential energy. An illustration of simplified MD simulations is shown in Figure 13.

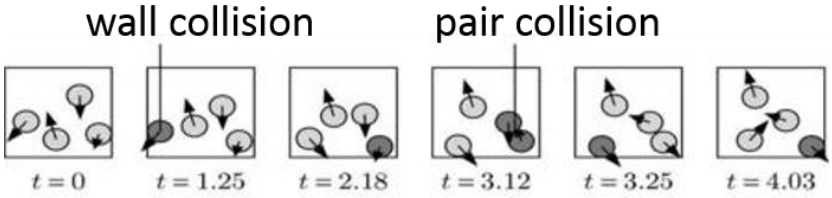

Source (StstMechAlgComp 2014)
Figure 13: Simplified MD simulations.

The forces on the particles are obtained from the gradient of potential energy which is usually described using the potential energy model for the inter-particle interactions (Wahnström 2013; Allen 2004). The force field is the set of parameters and equations that is used to describe the inter-particle interactions. The potential energy of a molecular system $U(\mathbf{r}^N)$can be represented as a sum of bonded (valence) interactions (U_{val}) and non-bonded interactions (U_{nb}) as (Mayo *et al.*, 1990; Allen 2004)

$$U(\mathbf{r}^N) = U_{\mathrm{val}}(\mathbf{r}^N) + U_{\mathrm{nb}}(\mathbf{r}^N). \tag{2}$$

The bonded interactions depend on the specific bonds of the structure, and the non-bonded interactions depend on the distance between the atoms (Mayo *et al.* 1990). Intramolecular bonding interactions (U_{val}) typically consist

of bond length/stretch (U_{bond}, two-body), bond-angle bend (U_{angle}, three-body), and dihedral torsion ($U_{dihedral}$, four-body) terms (Mayo *et al.* 1990; Allen 2004; Alexiadis and Kassinos 2008)

$$U_{val}(\boldsymbol{r}^N) = U_{bond}(\boldsymbol{r}^N) + U_{angle}(\boldsymbol{r}^N) + U_{dihedral}(\boldsymbol{r}^N), \tag{3}$$

while non-bonded interactions (U_{nb}) include long-range electrostatic forces (U_{q}) and shorter range dispersive (van der Waals) and repulsive overlap force (Pauli repulsion) interactions (U_{vdw}) (Mayo *et al.* 1990; Alexiadis and Kassinos 2008)

$$U_{nb}(\boldsymbol{r}^N) = U_{vdw}(\boldsymbol{r}^N) + U_q(\boldsymbol{r}^N). \tag{4}$$

A simplified graphical representation of these contributions to force potentials is shown in Figure 14.

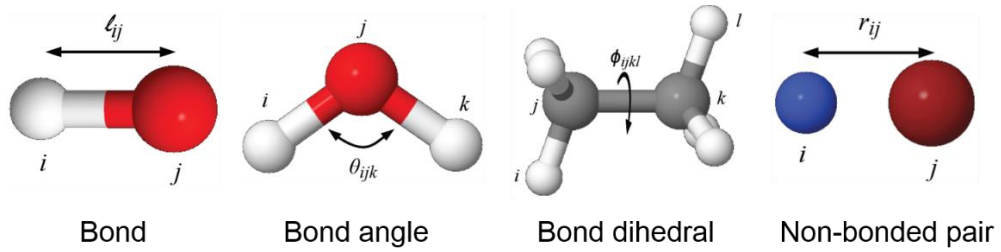

Source (Huang, 2013)
Figure 14: Illustration of bond-lengths, bond-angles and dihedral-angles and non-bonded pairs.

In this study, a second generation REBO (reactive empirical bond order) potential (Brenner *et al.* 2002), which is a complex potential involving 3-body interactions, was used to model the inter-atomic interactions between bonded atoms, and the non-bonded interactions between the atoms are described by a Lennard-Jones (LJ) 12-6 type potential (Carlborg *et al.*, 2008)

$$U(r_{ij}) = 4\varepsilon_{ij}\left[\left(\frac{\sigma_{ij}}{r_{ij}}\right)^{12} - \left(\frac{\sigma_{ij}}{r_{ij}}\right)^{6}\right], \tag{5}$$

where r_{ij} is the intermolecular distance between atoms i and j, and ε_{ij} and σ_{ij} are the Lennard-Jones parameters for the atoms. A graphical illustration of the Lennard-Jones potential is shown in Figure 15. A cut-off distance of r_c, beyond which the pair interaction is set to zero, is generally used to save computational time.

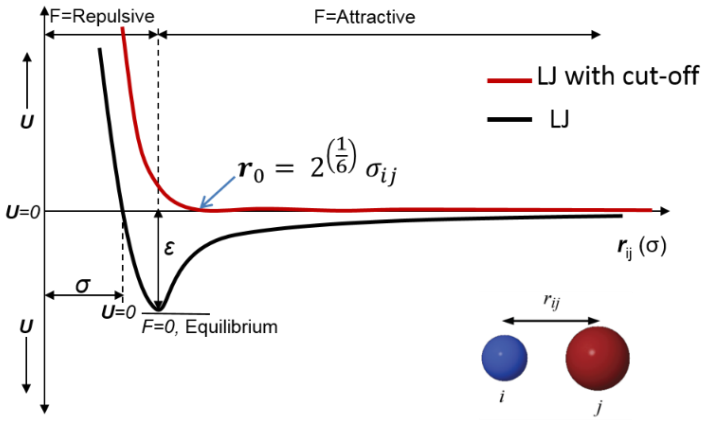

Source (Allen & Tildesley, 1989)
Figure 15: Graphical representations of Lennard-Jones potentials for non-bonded interactions between atoms.

4.1.2 MD model

A molecular system was designed to study acoustic wave propagation in a simple monatomic gas in a domain containing a 50 nm-long open-ended CNT cantilevered at the opposite to the sound source and parallel to the direction of the acoustic wave propagation. For simplicity, the simulation domain was modelled using monatomic argon gas as the wave propagation medium, a piston made of solid argon layers as a sound source, and a specular wall as the termination wall. An illustration of the modelled system is shown in Figure 16. The system was replicated in the transverse directions using periodic boundary conditions to create a system that represents an array of nanotubes or forest, which is similar to an experimental CNT array investigated in the authors' previous work (Ayub *et al.*, 2017). The intra-atomic interactions of non-bonded argon atoms and bonded carbon atoms were represented by LJ 12-6 potentials and REBO potentials, respectively. The inter-atomic interactions between argon and carbon atoms (argon-carbon) were also represented by a LJ potential (Carlborg *et al.*, 2008). A short-range purely repulsive WCA (Weeks-Chandler-Andersen) potential (Weeks *et al.*, 1971) with the same LJ parameters was used for the interaction between the atoms of the solid wall and those of the propagating medium (gas) by truncating the LJ potential at $2^{\frac{1}{6}}\sigma_{ij}$. Further details on the simulated system can be found in Ayub *et al.* (2018b). The total number of atoms in the simulation domain, N_{system} = 60,127 (with N_{wall} = 35,645, $N_{argon\ gas}$ = 20,402, $N_{free\ end\ CNT}$ = 3,990, and $N_{fixed\ end\ CNT}$ = 90) was constant during the simulations.

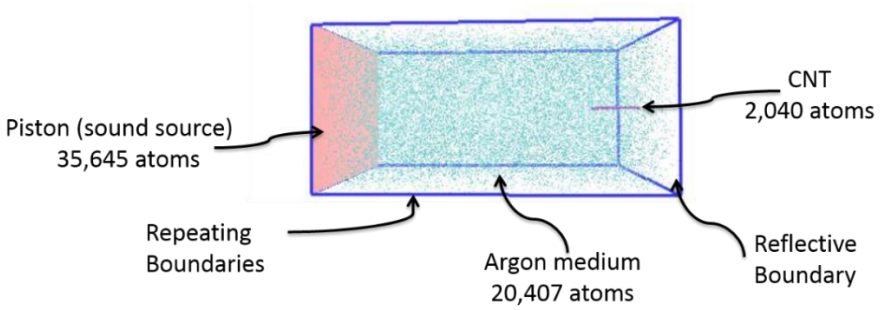

Figure 16: MD simulation domain with gas atoms in blue, CNT in purple (right) and atomistic piston in pink (left).

MD simulations were also performed without the CNT present for comparison. The characteristics of the acoustic field were studied by evaluating the behaviour of various acoustic parameters and comparing the change in behaviour with frequency. The attenuation of the acoustic wave was estimated using thermodynamic exergy concepts and compared against standing wave theory and predictions from continuum mechanics. Similarly, the acoustic field characteristics and attenuation due to the CNT were studied using MD simulations incorporating the CNT. A standing wave model, developed for the domain with the CNT present, was used to predict the attenuation by the CNT and verified against estimates from exergy concepts (Ayub *et al.*, 2018a; 2018b). Comparison of the simulation results for acoustic wave propagation with and without the CNT present demonstrated that acoustic absorption effects in the presence of CNTs can be simulated using the developed MD simulation setup although the degree of absorption was not sufficient for the CNTs simulated to investigate absorption mechanisms.

In order to estimate and demonstrate the dissipation of acoustic power in the simulation domain due to classical losses in the fluid medium, the estimate of total power flowing in the system is useful for power balance of system (Swift, 2002). The total power flowing in the wave-propagation direction can be related to the enthalpy in a moving gas using Rott's acoustic approximation (Swift, 2002), which gives the total power flux in this (z) direction as (Ayub *et al.*, 2018a; 2018b)

$$\dot{H}(z) = \frac{1}{2}\rho \int Re[hv^*]dA - (A\kappa + A_{solid}\kappa_{solid})\frac{dT_m}{dz}, \quad (6)$$

where $h\ (= U + PV = E_k + E_p + \frac{P}{\rho})$ is the enthalpy per unit mass, v^* is the complex conjugate of the particle velocity v, κ is the thermal conductivity, A is the cross-sectional area, T_m is the mean temperature of the gas and the subscript 'solid' denotes the properties corresponding to whatever solid is present in the system. The first term on the right side of Equation (6) is the time-averaged enthalpy flux and the second term is the conduction of heat

both in the gas and in the solid present in the system. Here, U is the sum of the total kinetic (E_k) and potential (E_p) energy, P is the pressure and V is the volume of the gas.

Figure 17 shows a comparison of estimates of total power (calculated using Equation (6) based on exergy concept) of the acoustic domain with and without the CNT present. It can be seen that the largest differences between the total power can be observed in the CNT region of the domain along the wave path of z >90 nm, indicating additional consumption of acoustic energy by the CNT compared with the CNT- free region. The modelled MD system can also be used to study deviations from continuum theory in the characteristics of high frequency sound. The study suggests that the investigation of absorption mechanisms in nanomaterials can be conducted using the developed platform for MD simulations, however further investigations are required to capture the loss mechanisms involved in the molecular interactions between the acoustic wave and the CNT. It should also be noted that due to the limited availability of computational resources, simulations were restricted to a relatively short and narrow CNT. In the work presented in this study, the analysis of a MD simulations of acoustic absorption by a single CNT in a small acoustic domain was considered, where typical solution times were on the order of 25 days (per 100 periods of the wave cycle) using 96 CPU cores of a supercomputer. Additionally, simulations were performed for the acoustic wave propagation at frequencies in the giga hertz range of 1.5 GHz to 2.5 GHz to reduce computational time. Hence, to permit simulations in the audible frequency range, it is necessary to speed up the computational process by modifying the system model such as by employing a hybrid model with molecular dynamics coupled to a continuum domain. Research has already been initiated by this group (Bennett *et al.* 2015) and is briefly described in the following section.

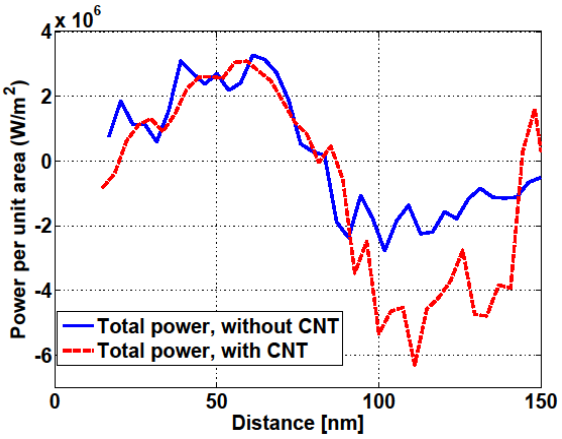

Figure 17: Comparison of total power in simulations with and without the CNT present.

4.2 Hybrid modelling: MD-FD

Previous work has investigated the effect of speedup techniques, such as multiple time-stepping and the use of an analytical sound source, on the computation speed of a MD nanomaterial-acoustic model (Bennett *et al.* 2015). Though significant speedup was obtained, it was insufficient to permit the modelling of audible frequencies. Hybrid modelling has the potential to assist the pursuit of simulations in the audible frequency range by ensuring the computationally expensive MD model is only applied in the regions where nanoscale features, such as nanomaterials, are present. The computational load is reduced by modelling the remainder of the domain with a more computationally efficient model. For a plane-wave system a one-dimensional finite difference (FD) model is appropriate. Since the minimum domain length scales with the inspected wavelength, hybrid modelling is particularly helpful when lower frequencies are investigated but the size of the nanoscale feature and hence, the MD subregion are maintained. The MD and FD sub-domains can be coupled to one another using an overlapping region as shown in Figure 18. In this overlapping region, the terminating cell of the FD scheme is controlled by the conditions of the coincident MD subregion, while an upstream MD subregion is controlled by an associated FD cell, as seen in Figure 18(b). This produces bi-directional coupling, which allows both incident and reflected acoustic waves to be transferred. Two acoustic parameters, such as velocity and density perturbation, are used in the coupling process to propagate the acoustic wave between the two subdomains, such that the combined systems act as if they were a single, extended domain.

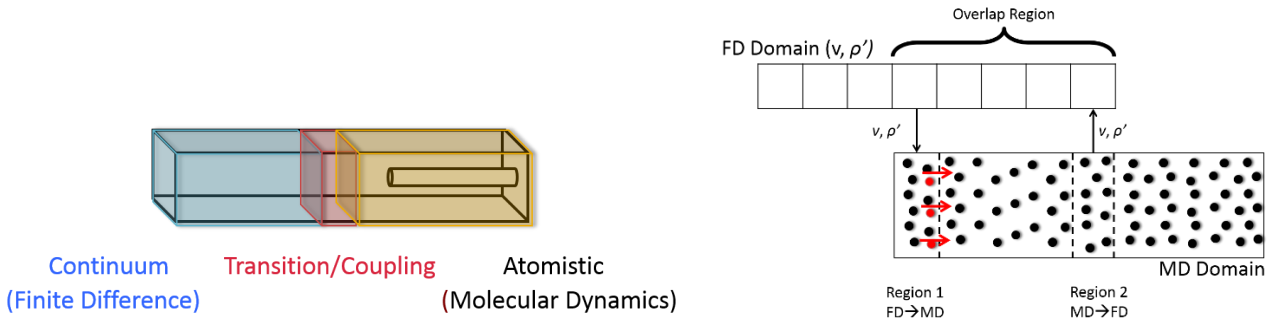

(a) Hybrid simulation domain (b) Coupling domain

Figure 18: Schematic of hybrid modelling domain separates a medium into continuum and atomistic regions.

5 CHARACTERISATION USING SEMI-PHENOMENOLOGICAL MODELS

The acoustic absorption mechanisms and the acoustic behaviour of CNTs are expected to differ with those of conventional porous materials based on considerations of the physical structure and size of the CNTs. Thus, the classical methods applicable for conventional materials might not be able to characterise the acoustic behaviour of the CNTs. Therefore, it is of interest to analyse the acoustic behaviour using classical methods to explore whether experimental estimates of the absorption coefficient of the CNTs deviate from theoretical predictions.

The simple empirical and classical methods of the Bies-Hansen (see Bies & Hansen (2003), p 623, Appendix C), Garai-Pompoli (2005) (both are actually a modified Delany-Bazley (1970) model), Biot-Allard (Biot, 1962; Allard, 1993) and Johnson-Allard (Allard, 1993) models were used to predict the acoustic absorption behaviour of the CNT forest. The non-acoustical parameters of the CNTs used here to calculate the theoretical acoustic absorption coefficient were estimated using theoretical models developed by Bies-Hansen (2003), Ballagh (1996), Garai-Pompoli (2005) and Allard-Champoux (1992). The geometrical and physical properties were measured by the research group in the Nanoworld Laboratories at the University of Cincinnati, USA, and the details have been presented previously (Ayub *et al.*, 2017). The predicted absorption coefficient of the CNT forest based on the estimated non-acoustical properties using the five theoretical methods is shown in Figure 19. It can be noticed that the predicted acoustic absorption coefficients are significantly influenced by the value of the estimated flow resistivity parameters. Consequently, it is also evident from Figure 19 that most of the classical methods based on phenomological models and microscopic mechanisms fail to accurately predict the acoustic absorption behaviour of the CNT forest. The reason for the discrepancies between the theoretical and experimental estimates of the acoustic absorption coefficient can be attributed to the significantly different values for the flow resistivity and characteristic lengths of the CNT forest compared with conventional materials. Compared with conventional porous materials, the estimated flow resistivity of the CNT forest is very high given the small thickness of the material. The large material density (43.4 kg m^{-3}) and the thin fibres (nanotube diameter = 12 nm) of the CNT forest, may contribute to the high flow resistivity, which influences the viscous and thermal losses substantially. As a result, CNTs may provide a different mechanism for structural vibration and heat transfer interaction with the gas molecules, which would contribute in a different manner to the viscous and thermal boundary layers of conventional materials. Thus, accurate estimates of the viscous and thermal effects during the interaction between the material and the sound wave would be crucial to predict the acoustic absorption of a CNT acoustic absorber.

Overall, it can be concluded that the microscopic absorption mechanism applicable to conventional materials is not applicable to nanoscopic fibres such as CNTs. In order to develop an understanding of the nanoscopic acoustic absorption mechanisms, acoustic modelling in the nanoscale range using molecular simulation is essential.

6 CONCLUSIONS

This paper presents an overview of recent research towards the development of acoustic absorbers using nanomaterials which involves investigating the absorption behaviour of carbon nanotube and graphene based acoustic absorbers, employing complex molecular techniques to understand the absorption mechanisms at the nanoscale. Investigations show that these nanomaterials have potential to be used as sound absorbing materials as they exhibit enhanced acoustic absorption performance over conventional materials and simultaneously provide beneficial properties of superhydrophobicity and fire-retardance. Implementation of classical semi-phenomenological

models to characterise the acoustic behaviour of nanomaterials indicate that the acoustic absorption mechanisms are likely to deviate from those for continuum phenomena and highlight the necessity of acoustic modelling at the nanoscale to develop an understanding of the nanoscopic absorption mechanisms of CNTs. Molecular dynamics (MD) simulation method was found to be useful to study the acoustic absorption mechanisms at the nanoscale. The developed MD simulation platform can be extended in the future to investigate the absorption effects of nanomaterials in the audible frequency range, potentially via a hybrid Finite Difference–Molecular Dynamics (FD-MD) approach.

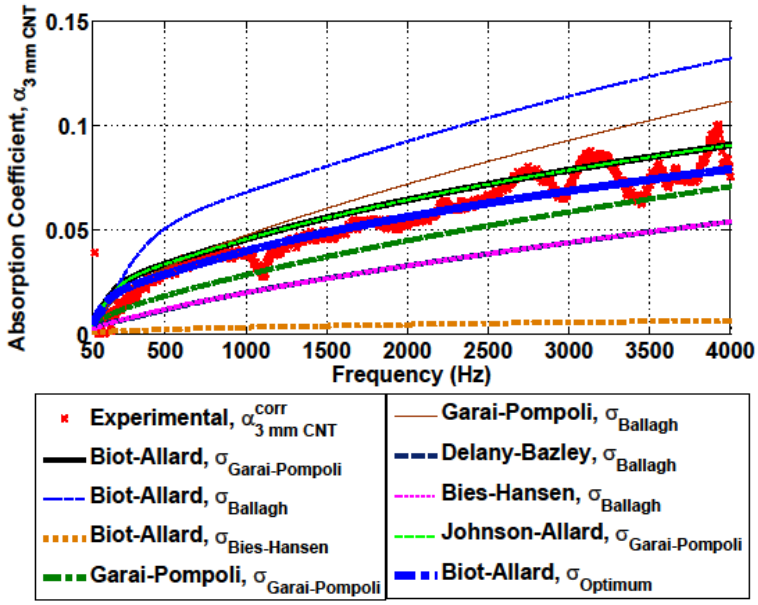

Figure 19: Theoretical prediction of the absorption coefficient of the CNT forest using the classical models of Biot-Allard (Allard, 1193; Hosseini Fouladi *et al.*, 2011), Johnson-Allard (Allard, 1993; Kino & Ueno, 2008) and Bies-Hansen (2003).

ACKNOWLEDGEMENTS

This research was supported under Australian Research Council's Discovery Projects funding scheme (project number DP130102832) and Interdisciplinary Research Funding 2018 by the University of Adelaide. This work was supported by computational resources provided by eResearchSA (https://www.ersa.edu.au/).

REFERENCES

Ajayan, P. *et al.* 2006. 'Carbon nanotube foam and method of making and using thereof'. US Patent No. 11/005474, Rensselaer Polytechnic Institute.

Alexiadis, A. and Kassinos, S. 2008. 'Molecular simulation of water in carbon nanotubes'. *Chemical Review* 108: 5014 –5034.

Allard, J. 1993. *Propagation of Sound in Porous Media: Modelling Sound Absorbing Materials*. Elsevier Applied Science, London.

Allard, J. F. and Champoux, Y. 1992. 'New empirical equations for sound propagation in rigid frame fibrous materials'. *Journal of the Acoustical Society of America* 91: 3346–3353.

Allen, M. P. 2004. *Introduction to molecular dynamics simulation/ Attig, N. et al. Computational Soft Matter: From Synthetic Polymers to Proteins*. 23: 1 –28.

Allen, M.P. and Tildesley, D.J. 1989. *Computer simulation of liquids*. Oxford: Oxford University Press.

Arenas, J. P. and Crocker, M. J. 2010. 'Recent trends in porous sound- absorbing materials'. *Sound & Vibration* 44 (7): 12-18.

ASTM E1050: Standard test method for impedance and absorption of acoustical materials using a tube, two microphones, and a digital frequency analysis system.1998. ASTM Internationals.

Ayub, M., Zander, A.C., Huang, D., Cazzolato, B. S., & Howard, C.Q. 2018a. 'Molecular dynamics simulation of classical sound absorption in a monatomic gas'. *Journal of Sound and Vibration* 421:319-333.

Ayub, M., Zander, A. C., Huang, D., Howard, C. Q., and Cazzolato, B.S. 2018b. 'Molecular dynamics simulations of acoustic absorption by a carbon nanotube'. *Physics of Fluids* 30(6): 066101.

Ayub, M. *et al.* 2017. 'Normal incidence acoustic absorption characteristics of a carbon nanotube forest'. *Applied Acoustics* 127: 223-229.
Ayub, M., Zander, A.C., Howard, C.Q. and Cazzolato, B.S. 2011. 'A review of acoustic absorption mechanisms of nanoscopic fibres'. In *Proceedings of Acoustics'11*, 77-84. Gold Coast, Australia.
Ayub, M., Zander, A.C., Howard, C.Q., Cazzolato, B.S. and Huang, D.M. 2013. 'A review of MD simulations of acoustic absorption mechanisms at the nanoscale'. In *Proceedings of Acoustics'13*, 19-26. Victor Harbor, Australia.
Ayub, M., Zander, A.C., Howard, C.Q., Huang, D.M. and Cazzolato, B.S. 2015. 'Molecular dynamics simulations of sound wave propagation in a gas and thermo-acoustic effects on a carbon nanotube'. *Journal of Computational Acoustics* 23(1540012):1-18.
Ballagh, K. 1996. 'Acoustical properties of wool'. *Applied Acoustics* 48(2): 101–120.
Bandarian, M. *et al.* 2011. 'Thermal, mechanical and acoustic damping properties of flexible open-cell polyurethane/multi-walled carbon nanotube foams: effect of surface functionality of nanotubes'. *Polymer International* 60(3): 475–482.
Basirjafari, S. *et al.* 2012. 'Low loading of carbon nanotubes to enhance acoustical properties of poly(ether)urethane foams'. *Journal of Applied Physics* 112(10): 104312.
Bennett, H. A., Zander, A. C., Cazzolato, B. S. and Huang, D. M. 2015. 'Speedup techniques for molecular dynamics simulations of the interaction of acoustic waves and nanomaterials'. In *Proceedings of the 21st International Congress on Modelling and Simulation (MODSIM2015)*, Queensland, Australia.
Bies, D. and Hansen, C. 2003. *Enginzeering Noise Control: Theory and Practice*. Third edition. Spon Press, London, UK.
Biot, M. 1962. 'Generalized theory of acoustic propagation in porous media'. *The Journal of the Acoustical Society of America* 34(9): 1254–1264.
Brenner, D. W. *et al.* 2002. 'A second-generation reactive empirical bond order (REBO) potential energy expression for hydrocarbons'. *Journal of Physics: Condensed Matter* 14(4): 783
Carlborg, C. F., Shiomi, J. and Maruyama, S. 2008. 'Thermal boundary resistance between single-walled carbon nanotubes and surrounding matrices'. *Physical Review B* 78: 1-8.
Cherng, J. 2006. 'Smart acoustic materials for automotive applications'. Technical report, Henry W Patton Center for Engineering Education and Practice, The University of Michigan-Dearnborn.
Cho, W. *et al.* 2014a. 'Growth and characterization of vertically aligned centimeter long CNT arrays'. *Carbon* 72: 264–273.
Cho, W. *et al.* 2014b. 'Growth termination mechanism of vertically aligned centimeter long carbon nanotube arrays'. *Carbon* 69: 609–620.
Chung, Y.J. & Blaser, D.A 1980a. 'Transfer function method of measuring in-duct acoustic properties. I. Theory'. *The Journal of the Acoustical Society of America* 68(3): 907–913.
Chung, Y.J. & Blaser, D.A. 1980b. 'Transfer function method of measuring in-duct acoustic properties. II. Experiment'. *The Journal of the Acoustical Society of America*, 68(3): 914–921.
Crawford, M. 2012. 'Reducing airplane noise with nanofibers'. <https://www.asme.org/engineering-topics/articles/aerospace-defense/reducing-airplane-noise-with-nanofibers>.
Crocker, M. J. and Arenas, J. P. 2007. *Use of Sound-Absorbing Materials, Chapter 57 in Handbook of Noise and Vibration Control/ M. J. Crocker*, John Wiley and Sons, New York.
Dedesko, S. and Siegel, J. A. 2015. 'Moisture parameters and fungal communities associated with gypsum drywall in buildings'. *Microbiome* 3:71.
Delany, M. E. and Bazley, E. N. 1970. 'Acoustical properties of fibrous absorbent material'. *Applied Acoustics* 3(2): 105 –116.
Fatima, S. and Mohanty, A. R. 2011. 'Acoustical and fire-retardant properties of jute composite materials'. *Applied Acoustics* 72(2-3): 108-114.
Fan, Z. *et al.* 2010. 'A three-dimensional carbon nanotube/graphene sandwich and its application as electrode in supercapacitors'. *Advanced materials* 22(33): 3723-3728.
Garai, M. and Pompoli, F. 2005. 'A simple empirical model of polyester fibre materials for acoustical applications'. *Applied Acoustics* 66:1383–1398.
Hadjiconstantinou, N. G. and Garcia, A. L. 2001. 'Molecular simulations of sound wave propagation in simple gases'. *Physics of Fluids* 13: 1040-1046.
Hadjiconstantinou, N. G. 2002. 'Sound wave propagation in transition regime micro- and nanochannels'. *Physics of Fluids* 14(2): 802 –809.
Han, J *et al.* 2007. 'Accurate measurement of small absorption coefficients'. Technical report, SAE Technical Paper 2007-01-2224. doi: 10.4271/2007- 01- 2224.
Hofmann, T. 2003. 'Molecular dynamics simulation of shock formation and reflection at a solid wall'. Diploma Thesis, ETH Zurich, Switzerland.
Hong, Z. *et al.* 2007. 'A novel composite sound absorber with recycled rubber particles'. *Journal of Sound and Vibration* 304(1-2): 400–406.
Hosseini Fouladi, M. *et al.* 2011. 'Analysis of coir fiber acoustical characteristics'. *Applied Acoustics* 72(1): 35–42.
Huang, D. M. 2014. 'Statistical mechanics and computer simulation of liquids'. Honours Chemistry Lecture notes, University of Adelaide, Australia.
Iijima, S. 1991. 'Helical microtubules of graphitic carbon'. *Nature* (London), 354:56-58.
Katz, B.F.G. 2000. 'Method to resolve microphone and sample location errors in the two-microphone duct measurement method'. *The Journal of the Acoustical Society of America* 108(5): 2231–2237.

Kino, N. and Ueno, T. 2008. 'Comparisons between characteristic lengths and fibre equivalent diameters in glass fibre and melamine foam materials of similar flow resistivity. *Applied Acoustics* 69: 325-331.
Kuczmarski, M. A. and Johnston, C. J. (2011) "Acoustic absorption in porous materials". NASA Technical Report, Ref. NASA/TM—2011-216995, Glenn Research Center, Cleveland, Ohio.
LDS Group 2013, LDS-Dactron RT Pro Dynamic Signal Analysis, User Guide, Rev. 7.10.
Leroy, P. *et al.* 2008. 'Smart foams for enhancing acoustic absorption'. In *Proceedings of Acoustics'08*. Paris, France.
Li, D. and Qiu, L. 2014. 'Graphene-based materials'. Patent WO2014028978 A1, Application No. PCT/AU2013/000939, Monash University.
Li, J. 2005. *Handbook of Materials Modeling/ S. Yip. Chapter 2.8 Basic Molecular Dynamics*, 565 –588, Netherlands: Springer.
Liu, Q. X. *et al.* 2012. 'Experimental and molecular dynamics study of gas flow characteristics in nanopores'. *Chinese Science Bulletin* 57: 1488–1493.
Liu, J., Xue, Y., Zhang, M. and Dai, L., 2012. 'Graphene-based materials for energy applications'. *Materials Research Society Bulletin* 37: 1265-1272.
Mayo, S. L. *et al.* 1990. 'DREIDING: A generic force field for molecular simulations'. *Journal of Physical Chemistry* 94: 8897–8909.
Mizuno, K *et al.* 2009. 'A black body absorber from vertically aligned single-walled carbon nanotubes'. In *Proceedings of the National Academy of Sciences*, 106(15): 6044-6047.
Nine, Md Julker, *et al.* 2017a. 'Graphene Oxide-Based Lamella Network for Enhanced Sound Absorption'. *Advanced Functional Materials* 27(46): 1703820.
Nine *et al.* 2017b.'Graphene-Borate as an Efficient Fire Retardant for Cellulosic Materials with Multiple and Synergetic Modes of Action'. *ACS Applied Materials Interfaces* 9(11): 10160-10168.
Oganov, A. R. *et al.* 2013. 'Structure, Bonding, and Mineralogy of Carbon at Extreme Conditions'. *Reviews in Mineralogy & Geochemistry* 75: 47-77.
Oh, J.H., Kim, J., Lee, H, Kang, Y., Oh I.K. 2018. 'Directionally Antagonistic Graphene Oxide-Polyurethane Hybrid Aerogel as a Sound Absorber'. *ACS Applied Material Interfaces* 10(26):22650-22660.
Qian, Y.J. *et al.* 2014. 'Improvement of sound absorption characteristics under low frequency for micro-perforated panel absorbers using super-aligned carbon nanotube arrays'. *Applied Acoustics* 82: 23 –27.
Robin, O., Berry, A., Doutres, O. and Atalla, N. 2014. 'Measurement of the absorption coefficient of sound absorbing materials under a synthesized diffuse acoustic field'. *The Journal of the Acoustical Society of America* 136 (1): EL13 – 19.
Robinson, R. 2008. 'Micro-Honeycomb Material Wears Out Engine Noise'. Georgia Tech Research Institute- Case study. url: http://gtri.gatech.edu/ casestudy/reducing-noise-micr-honeycomb.
Seetharamappa, J., Yellappa, S., DSouza, F. 2006. 'Carbon nanotubes: Next generation of electronic materials. *The Electrochemical Society Interface* 15(2):23-25.
StatMechAlgComp. 2014. 'Molecular Dynamics Simulation', image, StatMechAlgComp, viewed 20 October 2014, <https://statmechalgcomp.wikispaces.com/Hard_Spheres_MD_MC>.
Sun, X. *et al.* 2016. 'Graphene foam/carbon nanotube/poly(dimethyl siloxane) composites for exceptional microwave shielding'. *Composites: Part A* 85: 199-206.
Swift, G. W. 2002. *Thermoacoustics: a Unifying Perspective for Some Engines and Refrigerators*. Chap. 5, Sec. 5.2: 128–134. Acoustical Society of America, New York.
Tang, C. *et al.* 2014. 'Nitrogen-doped aligned Carbon nanotube/Graphene sandwiches: Facile catalytic growth on bifunctional natural catalysts and their applications as scaffolds for high-rate lithium-sulfur batteries'. *Advanced Materials* 26: 6100-6105.
Tiwari, A. and Syväjärvi, M., 2015. 'Graphene Materials: Fundamentals and Emerging Applications', John Wiley & Sons, May 4, Chapter 3, [in Architecture and Applications of Functional Three-dimensional Graphene Networks, by Dey, R. S. and Chi, Q.]
Turgut, H., Tian,Z. R., Yu, F. and Zhou, W. 2017. 'Multivalent Cation Cross-Linking Suppresses Highly Energetic Graphene Oxide's Flammability'. *The Journal of Physical Chemistry C* 121(10): 5829-5835.
Verdejo, R. *et al.* 2009. 'Enhanced acoustic damping in flexible polyurethane foams filled with carbon nanotubes'. *Composites Science and Technology* 69(10): 1564 –1569.
Viitanen, H. *et al.* 2009. Moisture and Bio-deterioration Risk of Building Materials and Structures'. *Journal of Building Physics* 33(3): 201-224
Wahnström, G. 2013. 'Molecular Dynamics'. Lecture Notes.
Weeks, J. D., Chandler, D. and Andersen, H. C. 1971. 'Role of repulsive forces in determining the equilibrium structure of simple liquids'. *Journal of Chemical Physics* 54: 5237-5247.
Xiao, L. *et al.* 2008. 'Flexible, stretchable, transparent carbon nanotube thin film loudspeakers'. *Nano letters* 8(12): 4539-4545.
Xu, M., Futaba, D.N., Yamada, T., Yumura, M., & Hata, K. 2010. 'Carbon nanotubes with temperature-invariant viscoelasticity from –196º to 1000ºC'. *Science* 330(6009): 1364-1368.
Zhang, L. *et al.* 2013. 'Porous 3D graphene-based bulk materials with exceptional high surface area and excellent conductivity for supercapacitors'. *Scientific Reports* 3(1408): 1-9.
Zhang, Q. *et al.* 2016. '3D printing of graphene aerogels'. *Small*, 12: 1702-1708.
Zhu, Y., Lei, L., Zhang, C., Casillas, Z. *et al.* 2012. 'A seamless three-dimensional carbon nanotube graphene hybrid material'. *Nature Communications* 3(1225): 1-7.